Hindawi
Advances in Materials Science and Engineering
Volume 2018, Article ID 9580526, 15 pages
https://doi.org/10.1155/2018/9580526

Research Article

Spatial and Temporal Distribution Law and Influencing Factors of the Mining-Induced Deformation and Failure of Gas Boreholes

Fei Xue [1,2] **and Xiaowei Feng** [3]

[1] *College of Civil Engineering, Shaoxing University, Shaoxing 312000, China*
[2] *Centre of Rock Mechanics and Geohazards, Shaoxing University, Shaoxing 312000, China*
[3] *Key Laboratory of Deep Coal Resource Mining, Ministry of Education of China, School of Mines, China University of Mining and Technology, Xuzhou 221116, China*

Correspondence should be addressed to Xiaowei Feng; fxw_mining@foxmail.com

Received 5 April 2018; Revised 12 June 2018; Accepted 8 July 2018; Published 15 August 2018

Academic Editor: Candido Fabrizio Pirri

Because gas boreholes are easy to damage by integrated coal mining and gas exploration, based on the practice of relieving pressure in deep thin coal seams in the Huainan mining area, a multidimensional coupling numerical simulation method was used to reveal the space-time evolution characteristics and influence factors of fracture deformation of gob-side gas boreholes. Results indicate that the danger zone for borehole fractures is primarily between 5 and 12 m above the roof of the roadway. The final-hole position has little effect on the stability of boreholes, and migrating the open-hole position to the entity coal side and roadway roof side can improve the stability of the borehole. The initial failure of the borehole occurs at a distance of 10 m behind the coal face. The failure of the borehole is largely stable at a distance of 100 to 120 m behind the coal face. With the increase in mining height, which leads to an increase in the movement of strata and an increase in pressure relief range, the shear stability of the borehole is reduced, and the extrusion stability of the borehole is improved. A hard roof condition promotes borehole shear stability, while a weak roof condition promotes borehole extrusion stability. This change can decrease the maintenance difficulty associated with "minor supports" in boreholes to a certain extent by reinforcing the support strength of "primary supports" in roadway retaining walls. The simulation results are consistent with observed results for the 11 test boreholes, and the accuracy of the numerical simulation is verified.

1. Introduction

Gas as a resource associated with coal is not only a type of clean energy but is also a dangerous source of energy that threatens safe mining practices in coal mines. How to extract gas safely and efficiently has always been a pertinent issue in coal mine safety in China [1]. The key technology of integrated pillarless coal production and methane extraction is a new gas extraction technology that was developed in recent years on the basis of pressure relief mining technology. According to the occurrence conditions of coal seams, the key layer is first exploited to carry out pressure relief, and then the gas extraction roadways arranged in the top/bottom rock stratum of the key layer were replaced by the gob-side retaining roadway [2]. The traditional U-shaped ventilation system was changed to a *Y*-type ventilation system, in which the pressure-relieved gas that was induced by the mining disturbance was continuously extracted by the drainage boreholes that were drilled behind the face in the gob-side retaining roadway.

The technology accounts for the safety and technical problems, including gas control, coal mining, roadway supports, ground temperature, and ground pressure control, and can realize safe and efficient integrated pillarless coal production and methane extraction [2]. However, due to the movement of strata and adjustments to stress in the rock strata above and below the panel after mining, the inclined cross-measure boreholes drilled in the retaining roadway suffered severe mining effects such that the extraction boreholes tend to fracture, and the gas extraction rate is poor. Dense extraction boreholes must be used in order to meet the requirements of gas extraction. Therefore, how to

maximize the drainage effect and reduce the drilling volume and construction cost is an urgent need to further achieve safe and efficient integrated coal production and methane extraction [3].

To improve the effect of borehole drainage, studies on the permeability of rock masses during mining and the seepage law of pressure-relieved gas have been conducted by various researchers, who have obtained abundant research results [4–10]. However, there has been less research focusing on the stability of boreholes, another factor that affects the effect of gas extraction, and existing literature primarily focuses on the mechanisms of surface venthole stability and protection technology. Whittles et al. investigated the effects that changes in the roof geology and roadway support system may have on deformation and closure of the gas drainage boreholes that are drilled from the tailgate across the gob of an active long wall panel. An analytical model was developed to estimate the bending deformation, axial strain, and the rupture of borehole casing due to rock shear and the optimum roadway support system, and the spacing between boreholes was also evaluated [11]. Liu et al. [12] conducted a stability analysis of surface ventholes based on the theory of surface subsidence and rock mechanics, which were also used to determine the borehole and casing diameters and the properties of casing fill materials. Sun et al. [13–15] established a shear and tensile failure model through a mechanical analysis and three-dimensional numerical simulation method, and the impact of the radius and thickness of the well casing, cement ring, and key stratum on borehole stability was investigated and verified in the field test. Chen et al. [16] analyzed the deformation and failure of a surface venthole casing under compression, tension, and shear conditions using numerical simulations. Périé [17] studied the failure characteristics of the surrounding rock of a gas extraction well using a field test, and it was demonstrated that the intermediate principal stress has an important influence on the stability of the gas well wall. Liu et al. [18] proposed that the structural design of the drilling well should be based on the properties of the formation. It is best to maintain a certain distance between the casing and the shaft wall. This approach not only can provide space for vertical compression and bending deformation of gas extraction wells but can also buffer the damage when horizontal displacement or deformation of the strata occurs, and the screen section of the gas drainage well should be strengthened.

The above studies used a variety of methods to analyze the stability of the surface ventholes from different angles, but due to significant differences in the layouts of inclined cross-measure boreholes that are drilled in the retaining roadway and surface ventholes, it is necessary to study the space-time evolution characteristics and main influence factors of fracture deformation of the gob-side borehole according to its layout characteristics in order to provide references for the design and protection of underground drainage boreholes.

2. Engineering Background

The Zhuji coal mine is located in the Huainan Panxie mining area and has an annual production capacity of 4 Mt/a. The coal mine has many complicated geological characteristics, such as large changes in the loose layer thickness, it is deeply buried, has a high gas content, a high in situ gas pressure, and a high geotemperature. At present, the coal mine mainly exploits the 11-2 and 13-1 coal seams. The 13-1 coal seam is a coal and gas outburst coal seam with an average gas content of 6.98 m^3/t, and gas content with such a high value can be seen in many literatures regarding gas drainage problems in the Huainan mining area, China [19, 20]. To eliminate the outburst danger of the 13-1 coal seam, the upper mining method was adopted to exploit the 11-2 coal seam firstly. The 1111(1) working panel is in the 11-2 coal seam. It has an average thickness of 1.26 m and an average dip angle of 3°, ranging from 1° to 5°. The mining height for the coal is 1.8 m, and the face elevation is -877.6 to -907.0 m with an average mining depth of 910 m. The panel length is 1612 m, and the panel width is 220 m. The working seam is overlain by seam 13-1, which is an outburst coal seam with a thickness of 4 m at a distance of 68 m. As shown in Figure 1, the face was mined using retreat longwall (LW) mining with full seam extraction, and the authors have conducted laboratorial trials regarding strengthening borehole configuration under identical engineering background [21]. It was ventilated using a *Y*-type ventilation system with the maingate and inlet part of the tailgate acting as the intake roadways and the outlet part of the tailgate and the floor return airgate acting as the return roadway. There were seven connection roadways (CR1~CR7) from the start line to the stop line between the tailgate and the floor return airgate. A 3 m wide concrete wall was constructed behind the LW face to replace the mined-out roadway wall along the gob side for building the retaining roadway.

During the mining of panel 1111(1), in order to prevent pressure-relieved gas of overlying coal seam 13-1 from entering into the working face and to eliminate the outburst danger of coal seam 13-1, a group of two inclined cross-measure boreholes were constructed at intervals of 25 m in the tailgate to extract the overburden pressure-relief gas. However, due to the redistribution of mining-induced stress and the overlying strata movement caused by the coal mining, deformation and failure associated with shear deformation, distortion, and extrusion appeared in the inclined cross-measure boreholes. The single-hole gas extraction flow was less than 0.3 m^3/min, and the effect of pressure-relief gas extraction could not be fully realized.

In view of the aforementioned engineering background, it is necessary to study the space-time evolution characteristics and main influence factors determining failure/deformation of the gob-side boreholes, and then some effective protection measures can be adopted to increase the stability of the borehole and extend the effective extraction time of the boreholes. Finally, the safe and efficient coal and gas simultaneous extraction can be realized.

3. Geological Model and Simulation Program

3.1. Deformation and Failure Form of Borehole. Three zones with different degrees of deformation were formed over the gob after mining (namely, the caved zone, the fractured

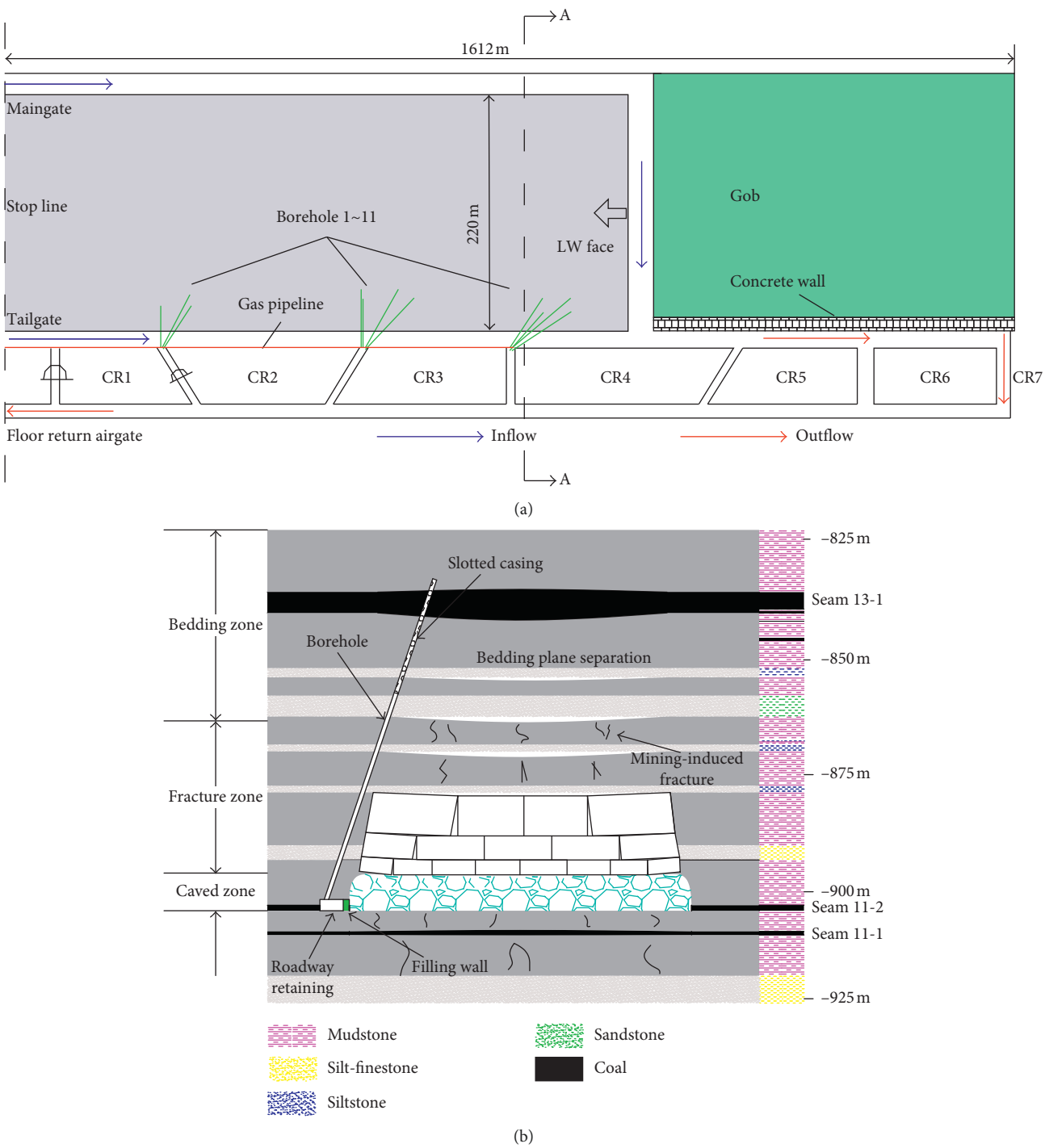

Figure 1: Panel 1111(1) and testing boreholes. (a) Plan view. (b) A-A section. The figure was reproduced from Xue et al. [21] (under the Creative Commons Attribution License/public domain).

zone, and the bending zone, as shown in Figure 1(a)), which were formed due to deformation of the overlying strata that occurs after the removal of panels. The deformation and failure modes of the gas drainage boreholes can be classified into two main categories: compressional failure resulting from concentrated compressive stresses both in the vertical and horizontal, and shear failure due to the dissimilarity of rock properties and incongruity of horizontal movement (shear offset) and longitudinal distortion between adjacent layers, as shown in Figure 2.

3.1.1. Rationale for Compressional Failure Mode. For the compressional failure mode, set borehole and strata as an integral research object (Figure 3), and assume that both of them are in elastic state, then in situ stress along the

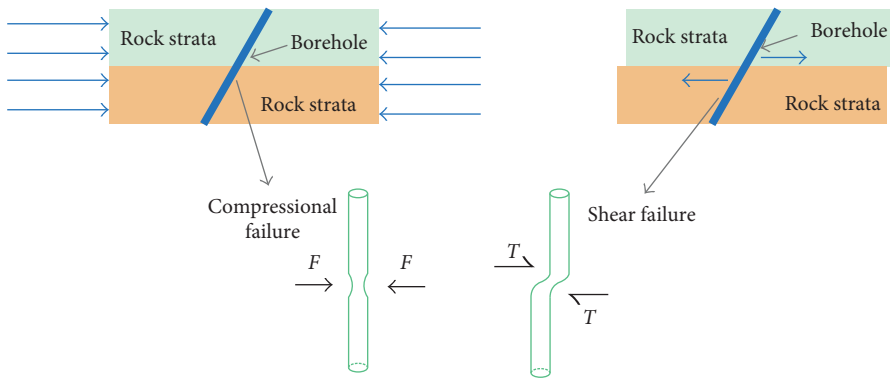

Figure 2: Schematic diagram of compressional and shear failure of a borehole induced by coal mining (modified from Liu et al. [24]).

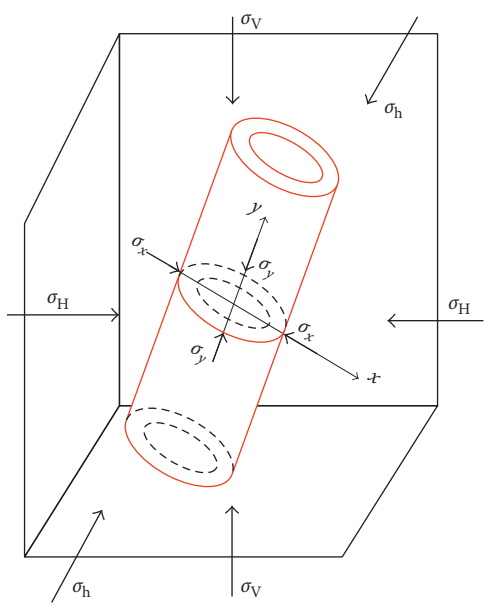

Figure 3: Sketch for mechanical model of casing under compression in strata.

cross-section direction of borehole is presented as follows based on elastic mechanics theory:

$$\begin{aligned} \sigma_x &= \left(\sigma_H \cos^2\alpha + \sigma_h \sin^2\alpha\right)\sin^2\beta + \sigma_v \cos^2\beta, \\ \sigma_y &= \sigma_H \sin^2\alpha + \sigma_h \cos^2\alpha, \end{aligned} \tag{1}$$

where α and β are azimuth angle and inclination of the borehole, respectively; σ_V, σ_H, and σ_h are vertical stress, maximum horizontal stress, and minimum horizontal stress of strata, respectively.

The extrusion force applied on the borehole can be represented by the sum of even load and uneven load, that is:

$$q = \frac{P_1 + P_2}{2} + \frac{P_1 - P_2}{2}\cos 2\theta, \tag{2}$$

where $P_1 = \max\{\sigma_x, \sigma_y\}$ and $P_2 = \min\{\sigma_x, \sigma_y\}$.

Afterwards, set casing as research object, based on the Von Mises yield criterion and adopt inverse formulation in elastic state, and then formula for ultimate extrusion strength of casing can be calculated by

$$P_c = \frac{-1.154\sigma_s}{\left(K_p + 1\right)A + \left(K_p - 1\right)\left(2A_1 + 6B + 6C + 2D\right)}, \tag{3}$$

where

$$\begin{aligned} A &= \frac{1}{1 - K_r^2}, \\ A_1 &= \frac{1}{2}\cdot\frac{1 + 3K_r^4 - 4K_r^6}{4K_r^2\left(1 - K_r^2\right)^2 - \left(1 - K_r^4\right)^2}, \\ B &= \frac{K_r^4\left(K_r^2 - 1\right)}{4K_r^2\left(1 - K_r^2\right)^2 - \left(1 - K_r^4\right)^2}, \\ C &= \frac{1}{2}\cdot\frac{1 - K_r^4}{4K_r^2\left(1 - K_r^2\right)^2 - \left(1 - K_r^4\right)^2}, \\ D &= \frac{K_r^6 - 1}{4K_r^2\left(1 - K_r^2\right)^2 - \left(1 - K_r^4\right)^2}, \\ K_r &= \frac{(r - t)}{r}, \\ K_p &= \frac{P_2}{P_1}, \end{aligned} \tag{4}$$

where σ_s is yield strength of casing, K_p is uneven coefficient of stress, and r and t are outer diameter and wall thickness of casing.

Based on the aforementioned theory, the safety factor of compressional failure of the borehole can be calculated according to (5). When the calculated value is less than 1, the borehole can be considered to be undergoing compressional failure:

$$f_c = \frac{P_c}{q_{max}}, \tag{5}$$

where f_c is the compressional safety factor of the borehole.

3.1.2. Rationale for Shear Failure Mode. For the shear failure mode, as shown in the right subfigure in Figure 2, "S" typed deformation of casing is generally observed under shearing

induced failure, and thus it can be roughly represented by sine function as [11]

$$u(y) = A\sin\left(\frac{2\pi y}{a}\right) \quad \left(0 < y < \frac{a}{2}\right), \tag{6}$$

where y is the distance along the borehole from shear plane (see Figure 4); $u(y)$ is the displacement at location y perpendicular to the y axis; A is amplitude of displacement; and a is wavelength (twofold value of the width of the shearing zone), which is closely correlated with mechanical properties and stress environment of strata.

In view of bending deformation principle in mechanics of materials, the bending-moment equation for the borehole casing under shear-slip deformation state is based on following equation:

$$M = \frac{4AEI\pi^2}{a^2}\sin\left(\frac{2\pi}{a}y\right) \quad \left(0 < y < \frac{a}{2}\right), \tag{7}$$

where E is elasticity modulus of casing.

Then the shear stress on the cross section of an annular girder is expressed by

$$\tau = \frac{QS_z^*}{I_z b} = \frac{8AE\pi^3}{3a^3}\cos\left(\frac{2\pi}{a}y\right) * \frac{(r^2-x^2)^{3/2} - \left[(r-t)^2 - x^2\right]^{3/2}}{(r^2-x^2)^{1/2} - \left[(r-t)^2 - x^2\right]^{1/2}}, \tag{8}$$

where Q is shear force acted on the cross section of the girder; S_z^* is static moment versus neutral axis for a section beyond x on the cross section, as shown by the shaded area in Figure 5, $S_z^* = (2/3)[(r^2-x^2)^{3/2} - [(r-t)^2 - x^2]^{3/2}]$; I_z is inertia moment of cross section versus neutral axis; r and t are outer diameter and wall thickness of the annular girder, respectively, $I_z = \pi[r^4 - (r-t)^4]/4$; and b is a value that doubles wall thickness, $b = 2[(r^2-x^2)^{1/2} - [(r-t)^2 - x^2]^{1/2}]$

Equation (8) shows shear stress of the borehole casing under shear-slip deformation state, therefore, the maximum shear stress on the cross section of casing can be expressed by

$$\tau_{\max} = \frac{8AE\pi^3(3r^2 - 3rt + t^2)}{3a^3}\cos\left(\frac{2\pi}{a}y\right). \tag{9}$$

In the same measure as mentioned above for compressional case, the shear failure safety factor of the borehole casing can be calculated according to (10). When the calculated value is less than 1, the borehole can be considered as undergoing shear failure:

$$f_s = \frac{\tau_{\lim}}{\tau_{\max}}, \tag{10}$$

where f_s is the shear safety factor of the borehole, $\tau_{\lim}$ is the shear strength of the casing, and $\tau_{\max}$ is the maximum shear stress of the the casing section. Detailed calculations for each parameter can be found in the literature [22].

3.2. Multidimensional Coupled Numerical Simulation Method. To obtain the characteristics of the macroscopic mining-induced stress distribution and stratal movement after coal mining, a 3D numerical model is usually adopted, note that there also have 2D FSDT and HSDT solutions besides 3D solutions. However, accounting for the accuracy of the simulation and the calculation of costs, as shown in Figure 6, the multidimensional coupled numerical simulation method was used to investigate the following. First, a large-scale 3D numerical model (larger grid size without considering the supporting effect) was constructed. The basic distribution law of the macroscopic mining-induced stress field and displacement field and the compaction rate of the gob at different places behind the coal face were obtained by 3D numerical simulation. Next, a 2D numerical model was used to further refine the grid and investigate the supporting effect. The distribution characteristics of the mining-induced

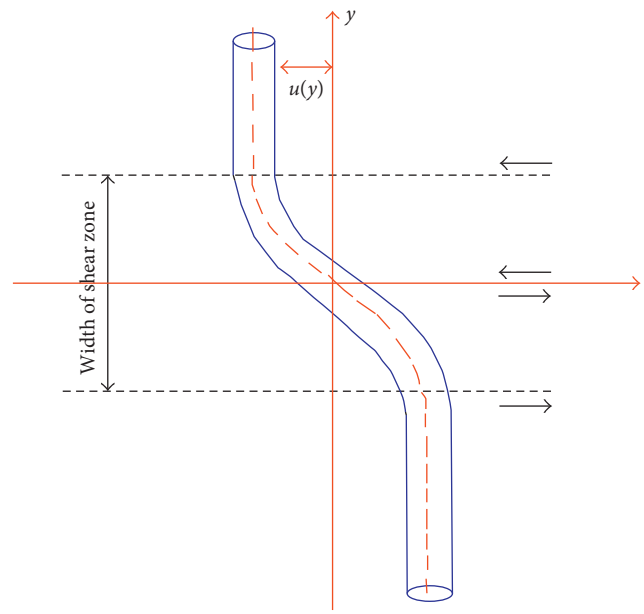

Figure 4: Sketch for "S" typed deformation of casing.

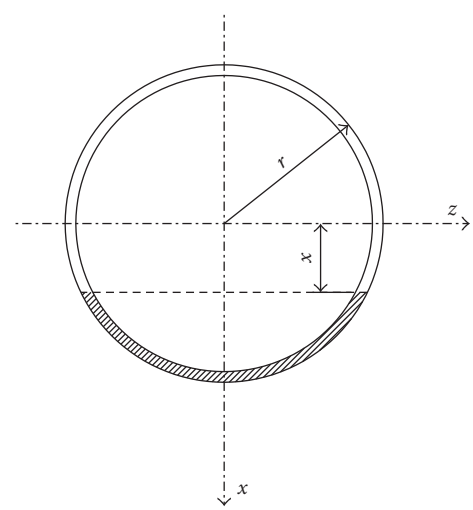

Figure 5: Sketch for mechanical analysis of the annular girder suffering shearing force.

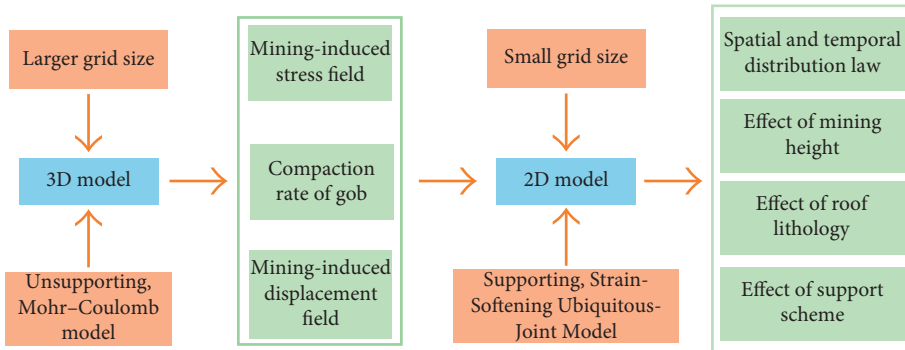

Figure 6: Schematic diagram for the multidimensional coupling numerical simulation method.

stress and the stratal movement in the cross section direction of the working face at different distances behind the coal face could be obtained by inversion according to the compaction rates of the gob at different distances behind the working face, which was obtained in the 3D simulation.

3.3. Model Design and Rock Parameters

3.3.1. Three-Dimensional Numerical Model. To eliminate the boundary effect and combine the engineering geology and mining technical conditions, as shown in Figure 7, the 3D model was scaled to 200 m wide, 200 m long, and 120 m high. The thickness of the coal seam, the roof strata, and the floor strata of the panel were 2.0 m, 98 m, and 20 m, respectively. The distribution of strata is shown in Table 1. Because of the symmetry of stratal movement in the working face, the 1/2 working face width (110 m) was simulated, and the simulated mining distance was 150 m. During the process of mining, a gob-side entry retaining roadway was implemented. The size of the retaining roadway was 4.0 m wide and 3.0 m high. The dimension of the concrete wall was 3 m wide and 3 m high. The model used a nonuniform grid. Small grids were used near the top and bottom floors of the coal seam. Large grids were used away from the mining area. The minimum grid size was 1 m × 1 m × 2 m, and the maximum grid size was 3 m × 4 m × 2 m. The entire model was divided into 750,000 units and 776,286 nodes. The upper boundary of the model was the stress boundary, at which an equivalent load of 20 MPa was applied. The remaining boundaries were displacement boundaries, and a normal displacement constraint was imposed.

3.3.2. Two-Dimensional Numerical Model. Similar to the 3D numerical model, only the size of the Y direction was set to 0.4 m. The mesh density was encrypted based on the 3D model. The minimum mesh size of the encrypted 2D model was 0.25 m × 0.25 m × 0.1 m. The total 2D model was divided into 367,820 units and 464,420 nodes. The model boundary conditions were the same as those used in the 3D model.

3.3.3. Constitutive Model and Rock Mass Parameters. Considering the simulation accuracy and computational cost, the 3D numerical model adopted the Mohr–Coulomb Model [23], whereas the 2D numerical model adopted the

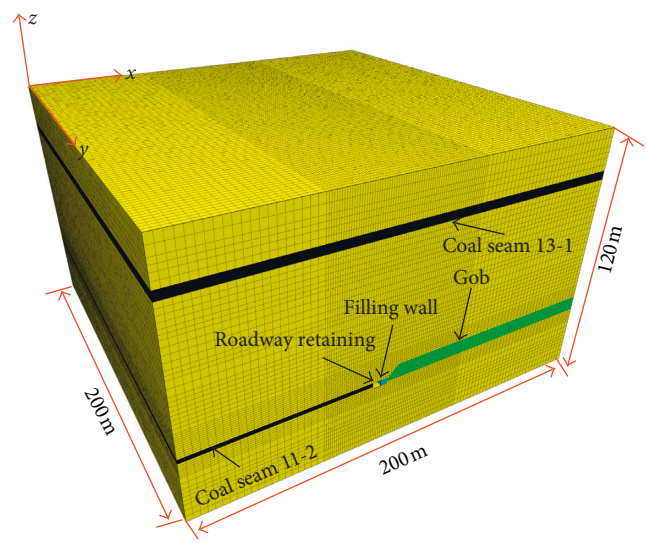

Figure 7: Dimension of numerical simulation model.

Table 1: Distribution of strata and their parameters in the basic model.

Number	Lithology	Thickness (m)	Total thickness (m)	Density (kg·m^{-3})
14	Sandstone	8	120	2800
13	Siltstone	5	112	2700
12	Mudstone	6	107	2400
11	Coalseam 13-1	4	101	1400
10	Mudstone	10	97	2400
9	Siltstone	4	87	2700
8	Mudstone	6	83	2400
7	Siltstone	6	77	2700
6	Sandstone	4	71	2800
5	Mudstone	7	67	2400
4	Sandstone	8	60	2800
3	Mudstone	8	52	2400
2	Sandstone	7	44	2700
1	Mudstone	5	37	2400
0	Coal seam 11-2	2	32	1400
−1	Mudstone	7	30	2400
−2	Siltstone	6	23	2700
−3	Mudstone	8	17	2400
−4	Siltstone	9	9	2700

Strain-Softening Ubiquitous-Joint Model, which could not only consider the stress-strain relationship of the material after peak but could also meet the needs of the analysis of joints and weak surfaces. Detailed rock mass parameters are shown in Table 2.

3.4. Simulation Program. The coal seam excavation was excavated along the coal seam direction (Y direction) step-by-step in the 3D numerical simulation. Each excavation distance was 10 m, and a total of 150 m was excavated. After excavation, the monitoring lines were arranged along the Y direction at $x = 200$ and $z = 29$ to extract the compaction rate of the gob area at different distances behind the coal face, which provided an inversion basis for the 2D model to analyze the deformation and failure rules of drainage boreholes at different distances behind the coal face.

The coal seam excavation was excavated in one step in the 2D numerical simulation. To obtain the spatial distribution law of the deformation and failure of the drainage boreholes, as shown in Figure 8, a total of nine sets of drilling paths were designed. The initial location of the 1# through 3# drilling paths was $x = 80$ m and $z = 32$ m, and the final location was $x = 110$ m, 120 m, 130 m, and $z = 97$ m, respectively. The final location of the 4# through 9# drilling paths was $x = 120$ m and $z = 97$ m, and the initial location was $x = 80$ m, $z = 37$ m, 42 m, 47 m and $x = 83$ m, 86 m, 77 m, and $z = 32$ m, respectively. At the same time, according to the compaction rate of the gob area at different distances behind the coal face obtained from 3D simulation, the dynamic evolution rule of the drainage borehole deformation and failure behind the coal face was retrieved from the subsidence of the roof node of the caving zone.

To obtain the influence rule of different mining heights and roof properties on drainage borehole stability, three mining heights (2 m, 3 m, and 4 m) and three roof conditions (a common roof with 5 mudstone and 7 m sandstone, a hard roof with 12 m sandstone, and a soft roof with 12 m mudstone) were designed.

To obtain the influence law of different support conditions on the stability of the drainage boreholes, as shown in Table 3, a total of three types of supports were designed. The cable unit in FLAC3D was used to simulate rock bolts and cables. The size of the bolt and cable was $\Phi 22 \times 2000$ mm and $\Phi 21.8 \times 6000$ mm, and the mechanical parameters of the bolt and cable are shown in Table 4. The concrete wall was simulated with three kinds of strength, and the strength parameters are shown in Table 5.

Considering the aforementioned factors, a total of seven sets of simulation schemes were designed, and the detailed simulation schemes are shown in Table 6.

4. Analysis and Discussion of Model Results

4.1. Compaction Rate of Gob at Different Distances behind the Coal Face. The subsidence ratio of the gob roof at different distances behind the coal face is shown in Figure 9. The transverse coordinates in Figure 9 indicate the distance from the coal face. A positive value represents an area behind the coal face, and a negative value represents the front of the coal face. Due to the fragmental dilatancy of caving rock in the gob, the compaction rates of the caving rock in the gob at different distances behind the coal face are different; therefore, the ratios of the subsidence of the gob roof are different. Therefore, the ratio of subsidence of the gob roof can be used to characterize the compaction rate of the caving rock in the gob behind the coal face. It can be concluded from Figure 9 that the compaction rate of the caving rock at the position of the coal face is approximately 24%, and with an increase in the distance behind the coal face, the compacting rate of the caving rock in the gob also increases. The compacting rate of the caving rock is nearly 100% at a position 120 m behind the coal face. It can be concluded that the mining influence will tend to be stable behind the coal face at 120 m, which is consistent with the field measured value of panel 1111(1) in the Zhuji coal mine. Therefore, the correctness of the numerical simulation is verified.

4.2. Spatial Distribution Law of Drainage Borehole Deformation and Failure. Assuming that protective casing of the drainage boreholes is $\Phi 89 * 8$ mm N80 oil casing, the critical shear slip of the borehole casing can be calculated to be 0.01 m according to the literature [24]. The displacement and stress of each node in the three-dimensional model can be extracted, and the shear slip and the compressional safety factors at different locations of each drilling path can be obtained.

The shear slip and compressional safety factor distribution curves of the 1# through 9# drilling paths are shown in Figure 10. The red dashed line represents the critical shear slip of the drainage boreholes, and the blue dashed line represents the critical compressional safety factor of the drainage boreholes.

Comparing the distribution of shear slip and compressional safety factors of the 1# through 3# drilling paths in Figure 10, the effect of the final location on the stability of the drainage boreholes can be obtained. The dangerous regions of shear and compressional failure of the drainage boreholes are both mainly located at a position near the final location of the boreholes. The dangerous regions of the shear failure of the drainage boreholes are mainly located in strata above the roadway roof between 1–12 m, 18-19 m, 21–27 m, and 30–32 m. The interlayer shear slip in the strata above the roadway roof at 1–5 m is the most dramatic with a maximum shear slip of 0.08 m, and the shear slip in the region above the roadway roof at 32 m is smaller. The dangerous regions of the compressional failure of the drainage boreholes are mainly located in strata above the roadway roof at 5–11 m. With the migration of the final location to the gob side, the dangerous regions and the risk degree of the compressional failure are gradually reduced. Therefore, the final location of the drainage boreholes has little influence on borehole stability. The final location of the drainage boreholes can be migrated to the gob side in the drilling design so that the borehole can pass through the high gas penetration zone to achieve the best extraction effect.

Comparing the distribution of shear slip and compressional safety factors of the 4# through 6# drilling paths in Figure 10, the effect of the vertical distance between the

Table 2: Mechanical parameters of strata.

Lithology				Coal	Mudstone	Siltstone	Sandstone
Strength parameters	Matrix	Peak value	Internal friction (°)	29	35	45	50
			Cohesion (MPa)	1.06	1.9	2.2	2.8
			Tensile strength (MPa)	0.03	0.42	0.68	1
		Residual value	Internal friction (°)	28	34	43	48
			Cohesion (MPa)	0.0106	0.19	0.22	0.28
			Tensile strength (MPa)	0	0	0	0
	Joint	Peak value	Internal friction (°)	25	30	42	45
			Cohesion (MPa)	0.8	1.5	2	2.5
			Tensile strength (MPa)	0.01	0.4	0.6	0.8
		Residual value	Internal friction (°)	24	29	38	43
			Cohesion (MPa)	0.008	0.15	0.2	0.25
			Tensile strength (MPa)	0	0	0	0
Stiffness parameters	Bulk modulus (GPa)			1.5	3.5	3.6	5.3
	Shear modulus (GPa)			0.3	1.6	2.2	4

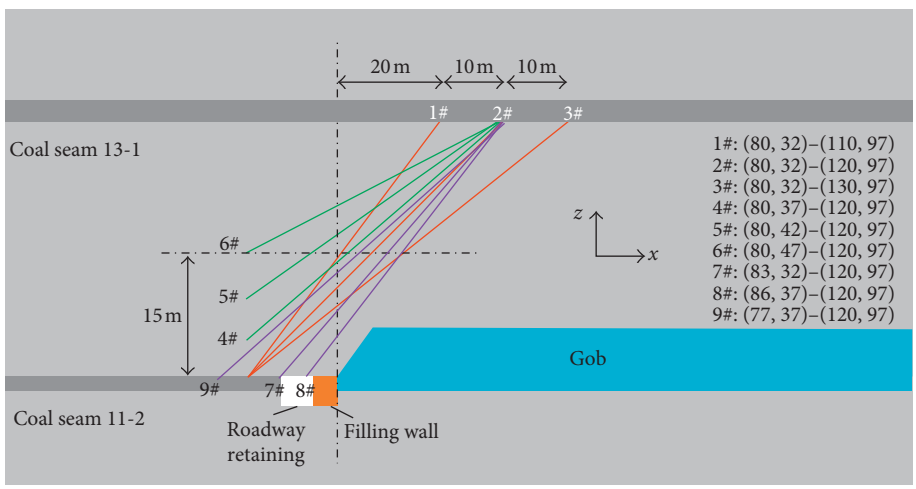

Figure 8: Schematic diagram for the location of the drainage boreholes in the 2D model. Coordinates attached on the right section indicate initial location and final location for each drilling path.

Table 3: Three different support schemes.

Supporting scheme	Roadway roof	Roadway sidewall on nonmining side	Filling zone roof	Filling wall
1	Seven bolts	Seven bolts	None	C20
2	Seven bolts + three cables	Seven bolts + two cables	Three bolts	C30
3	Seven bolts + seven cables	Seven bolts + three cables	Three bolts + three cables	C40

Table 4: Material parameters for bolts and cables.

	Elasticity modulus (GPa)	Cross-sectional area (m^2)	Grout cohesion (kN/m)	Grout stiffness (GPa)	Ultimate tensile capacity (kN)	Pretensile (kN)
Bolt	200	0.00038	1400	0.11	152	80
Cable	200	0.00038	1400	0.11	700	120

Table 5: Parameters for backfilling wall materials.

	Density ($kg{\cdot}m^{-3}$)	Bulk modulus (GPa)	Shear modulus (GPa)	Cohesion (MPa)	Internal friction (°)	Tensile strength (MPa)
C20	2000	2.2	0.9	3	20	0.75
C30	2300	2.4	1.3	4.2	22	1.05
C40	2500	2.7	1.7	5.4	24	1.35

Table 6: Simulation schemes.

Number	Mining height (m)	Roof lithology	Support scheme
1	2	Common roof	1
2	3	Common roof	1
3	4	Common roof	1
4	2	Hard roof	1
5	2	Soft roof	1
6	2	Common roof	2
7	2	Common roof	3

initial location of the boreholes with the roadway roof on the stability of the drainage boreholes can be obtained. Due to the upward shift of the initial location of the drainage boreholes, severe shearing and sliding in the strata above the roadway roof at 1–5 m is avoided. The shear slip of strata is significantly reduced with a maximum shear slip of 0.03 m, and the risk degree of borehole shear failure is significantly reduced. With an increase in the vertical distance between the initial location of the boreholes with the roadway roof, the dangerous area and the risk degree of the boreholes shear failure are reduced. Similarly, with an upward shift of the initial location of the drainage boreholes, severe compression in the strata above the roadway roof at 5–11 m is avoided. The dangerous area and the risk degree of borehole compressional failure are also reduced.

Comparing the distribution of shear slip and compressional safety factors of the 7# through 9# drilling paths in Figure 10, the effect of the horizontal distance between the initial locations of the boreholes with the filling wall on the stability of the drainage boreholes can be obtained. With a decrease in the distance between the initial locations of boreholes with the filling wall, the dangerous area of the borehole shear failure is basically unchanged, but the risk degree of shear failure increases significantly. When the horizontal distance between the initial locations of boreholes with the filling wall is 10 m, the maximum shear slip of boreholes is only 0.026 m. When the horizontal distance between the initial location of boreholes with the filling wall is 4 m, the maximum shear slip of boreholes reaches 0.17 m, which is 6.5 times that of the former. Therefore, the dangerous area of the borehole shear failure is mainly located in the 5 m of strata above the roadway roof, and the lower the layer, the greater the shear slip. As the horizontal distance between the initial locations of boreholes with the filling wall decreases, the danger area and risk degree of the borehole compression failure are slightly reduced, which indicates that the dangerous area of the borehole compressional failure is primarily located in the region near the sidewall on the nonmining side.

4.3. Temporal Distribution Law of the Deformation and Failure of Boreholes. According to the subsidence ratio of the gob roof at different distances behind the coal face in the 3D model, the evolution rule of the dangerous area and risk degree of the borehole with the advance of the coal face can be retrieved by monitoring the subsidence value of the gob roof node in the 2D numerical model. The evolution law of the shear and compressional stability with advance of the coal face of the 2# drilling path is shown in Figure 11. From Figure 11, it can be concluded as follows:

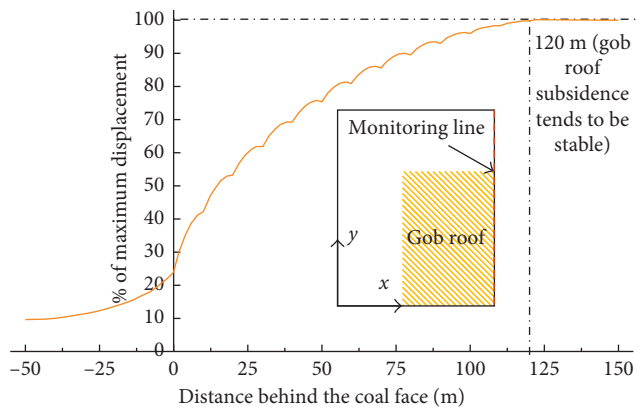

Figure 9: Roof subsidence curve at different distances behind the coal face.

(1) The shear slip of the borehole increases approximately linearly with the increase in distance behind the coal face. The shear slip and growth rate of lower strata are significantly higher than those of upper strata, especially in the strata above the roadway roof at 5 m. The time of borehole shear failure initially occurred at a distance of 10 m behind the coal face, and with continuous advance of the coal face, the dangerous area and risk degree continued to increase until it was basically stable at a distance of 120 m behind the coal face.

(2) The safety factor of borehole compressional failure gradually decreases with the advance of the coal face as a whole. The mining-induced stress adjustment of lower strata is less than that of upper strata, and the time to reach stability is also shorter than for upper strata. The mining-induced stress adjustment at a depth of 6 m along the borehole is basically stable at a distance of 60 m behind the coal face. The mining-induced stress adjustment at a depth of 60 m along the borehole still has greater adjustment at a distance of 60 m behind the coal face. This shows that the stress adjustment is lagging in the upper strata. The time of borehole compressional failure initially occurred at a distance of 10 m behind the coal face, and compressional failure occurred again in the upper strata at a distance of 70 m behind the coal face. The compressional failure of the borehole was basically stable at a distance of 100 m behind the coal face.

4.4. Effect of Mining Height on the Stability of Boreholes. The variation rules of the borehole stability of the 2# drilling path with mining heights of 2 m, 3 m, and 4 m are shown in Figure 12. It is concluded from the diagram as follows:

(1) With an increase in mining height, the dangerous area of the borehole shear failure also increases and is primarily concentrated in the upper strata at 20 m

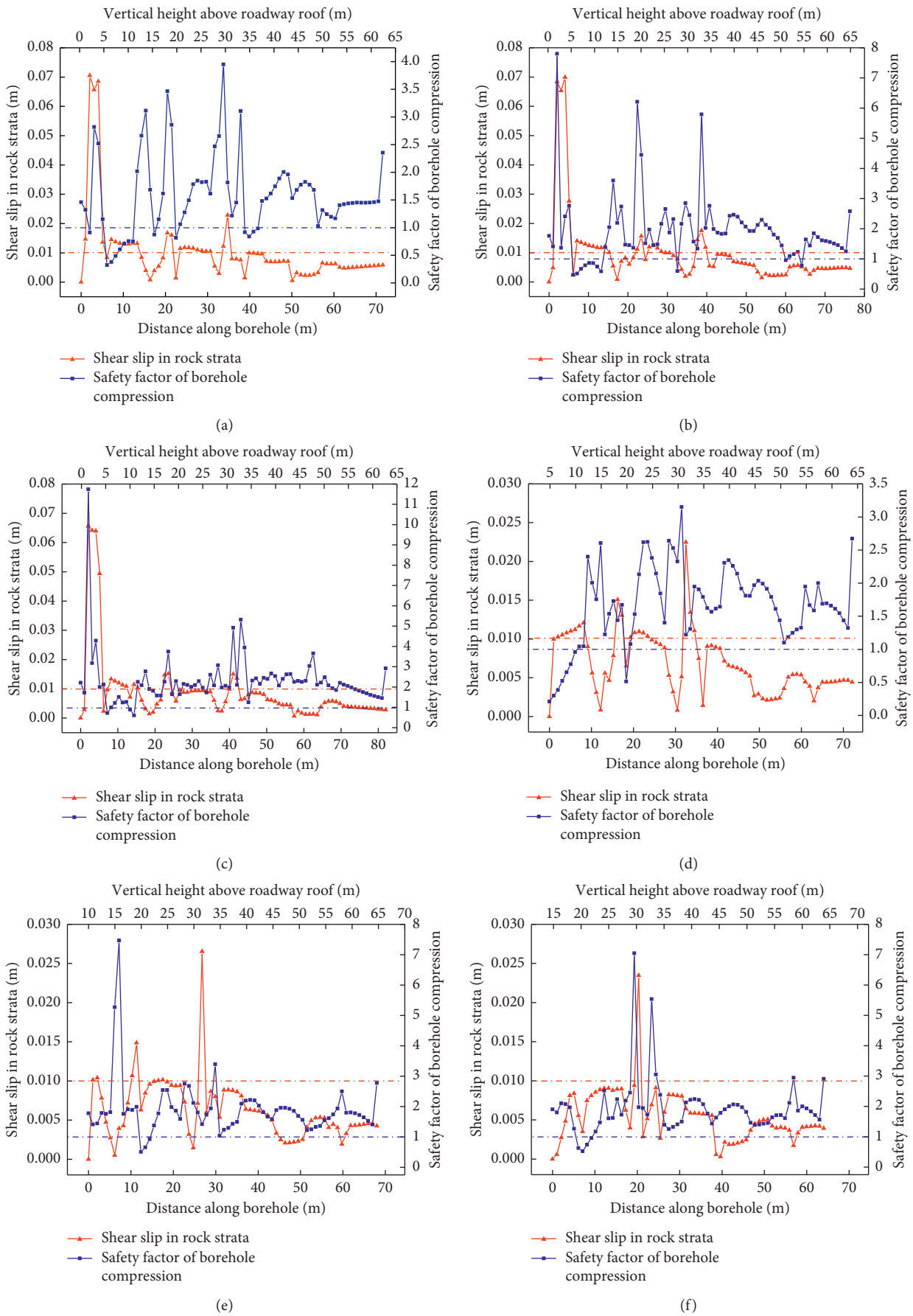

Figure 10: Continued.

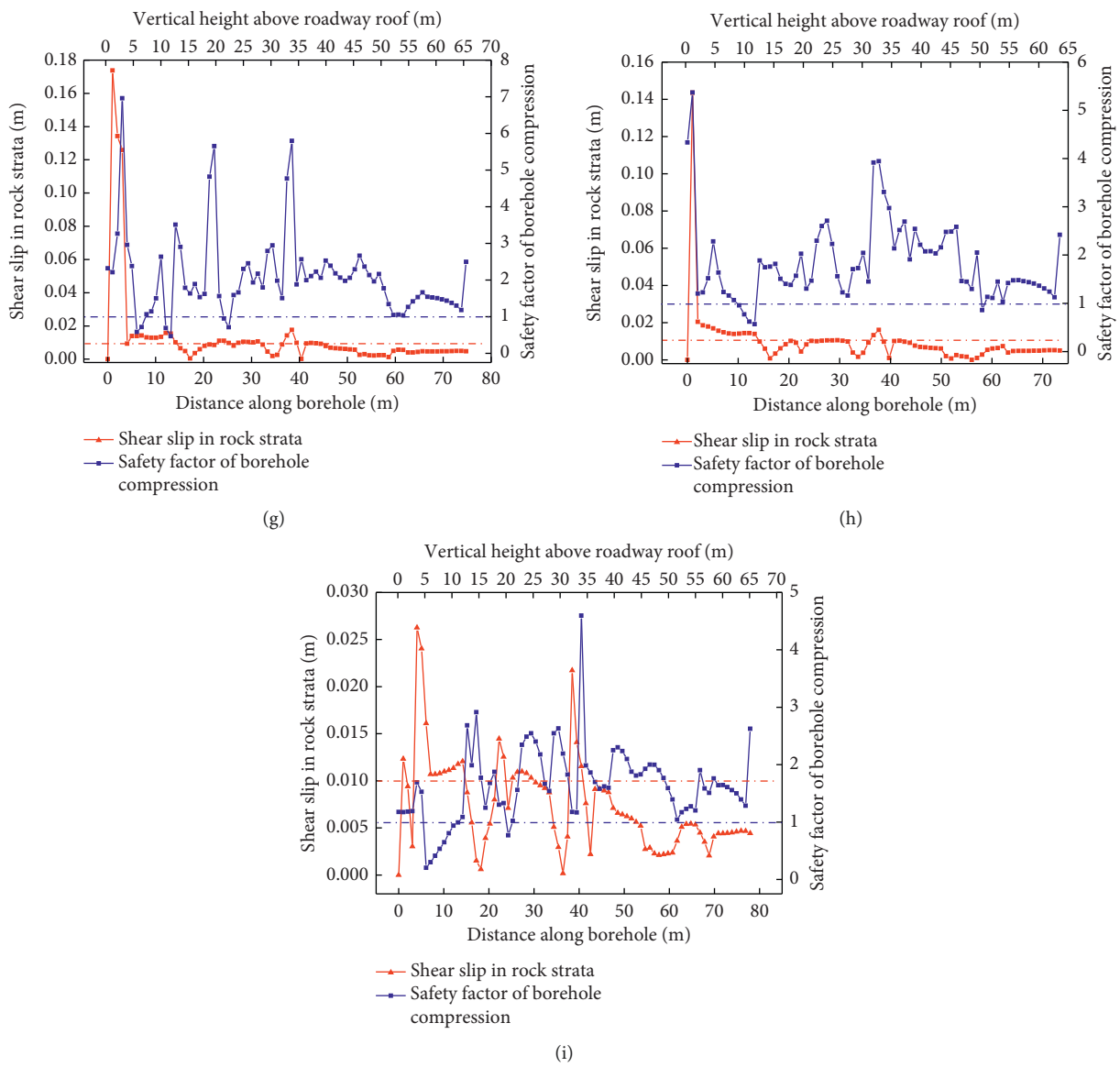

Figure 10: Distribution law for shear-slippage value and compressional safety factor in the 1 through 9# drilling paths. (a) 1# drilling path, (b) 2# drilling path, (c) 3# drilling path, (d) 4# drilling path, (e) 5# drilling path, (f) 6# drilling path, (g) 7# drilling path, (h) 8# drilling path, and (i) 9# drilling path.

depth along the borehole. In addition, shear slip decreases in the lower strata below 20 m depth along the borehole. This indicates that the increase in mining height mainly results in an increase in the displacement of upper strata, whereas lower strata are less affected by the mining height due to the supporting effect of the filling wall.

(2) As the mining height increases, the dangerous area and risk degree of borehole compressional failure reduced. This is due to the increase in mining height, which results in an increase in the pressure relief range that is caused by mining.

4.5. Effect of Roof Lithology on Borehole Stability. The variation rules of the borehole stability of the 2# drilling path with the roof lithologies including a common roof, a hard roof, and a soft roof are shown in Figure 13. We conclude the following from the diagram:

(1) The hard roof conditions are most favorable to shear stability of the borehole, and the soft roof conditions are the second most favorable. When the roof lithology is a hard roof, the subsidence of the lateral roof obviously decreases due to the high strength and stiffness of the roof, especially in lower strata, such that the shear slip of a hard roof is lower than that of other types of roofs. When the roof lithology is a soft roof, stratal movement is lower than for the common roof condition due to the dilatancy of the soft roof, and the shear slip of the soft roof is lower than that of the common roof.

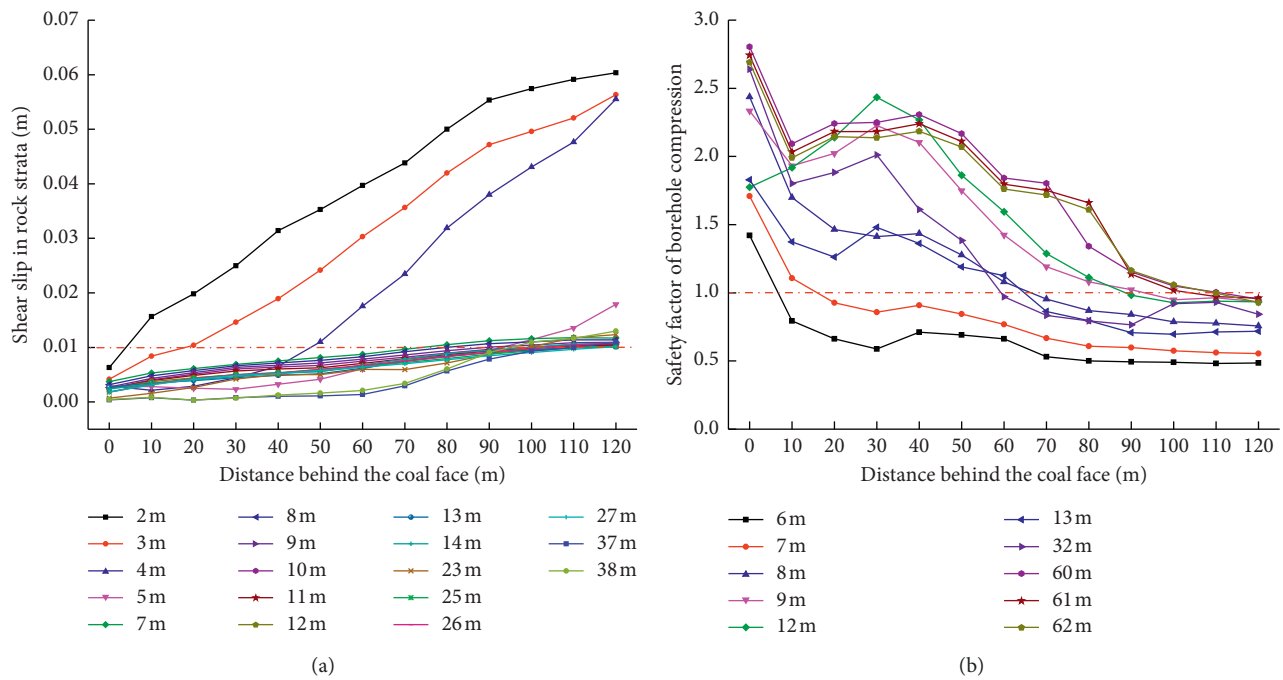

Figure 11: Evolution laws for the stability of the borehole with advance of the coal face. (a) Evolution of the dangerous location and shear slip of the borehole with advance of the coal face. (b) Evolution of the dangerous location and safety factor of borehole compressional failure with advance of the coal face.

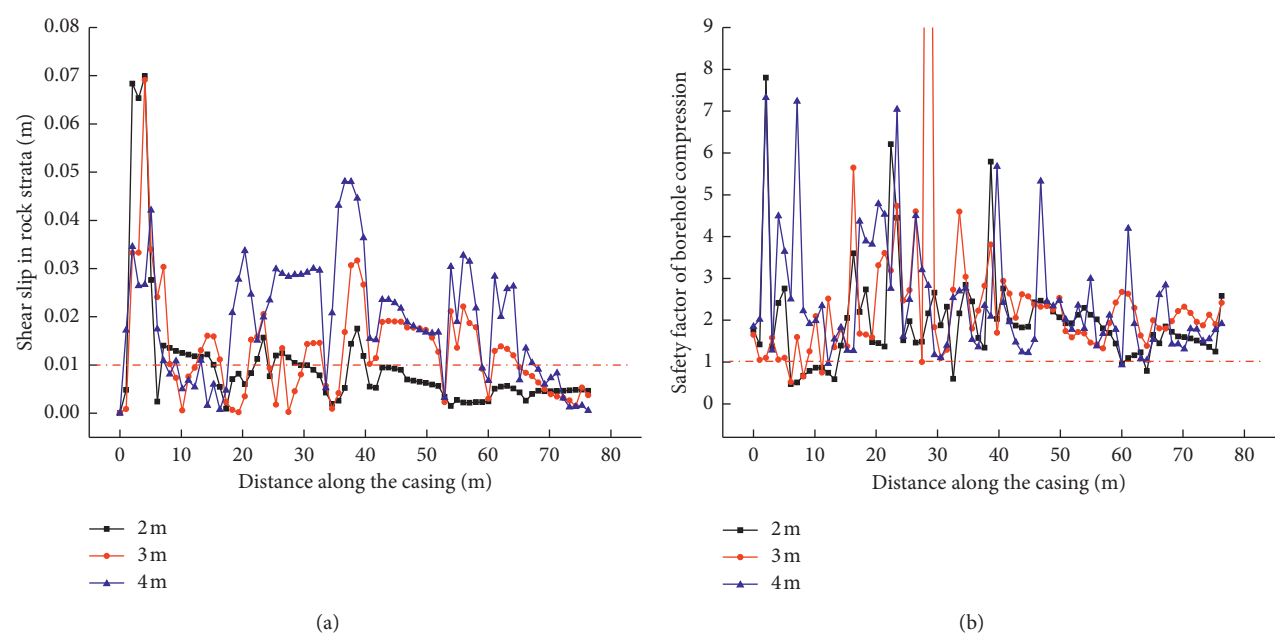

Figure 12: Effect of mining height on the stability of the borehole. (a) Effect of mining height on the shear stability of the borehole. (b) Effect of mining height on the compressional stability of the borehole.

(2) The soft roof conditions are most favorable to compressional stability of the borehole, and the hard roof is the second most favorable. When the roof lithology is a hard roof, the concentration of horizontal stress in the lateral lower strata of the gob is higher than that of the common roof, such that it is easy to form a dangerous area of compressional failure in the lower strata. When the roof lithology is a soft roof, the mining disturbance effect is lower than for the common roof, and the dangerous area of the compressional failure is significantly reduced.

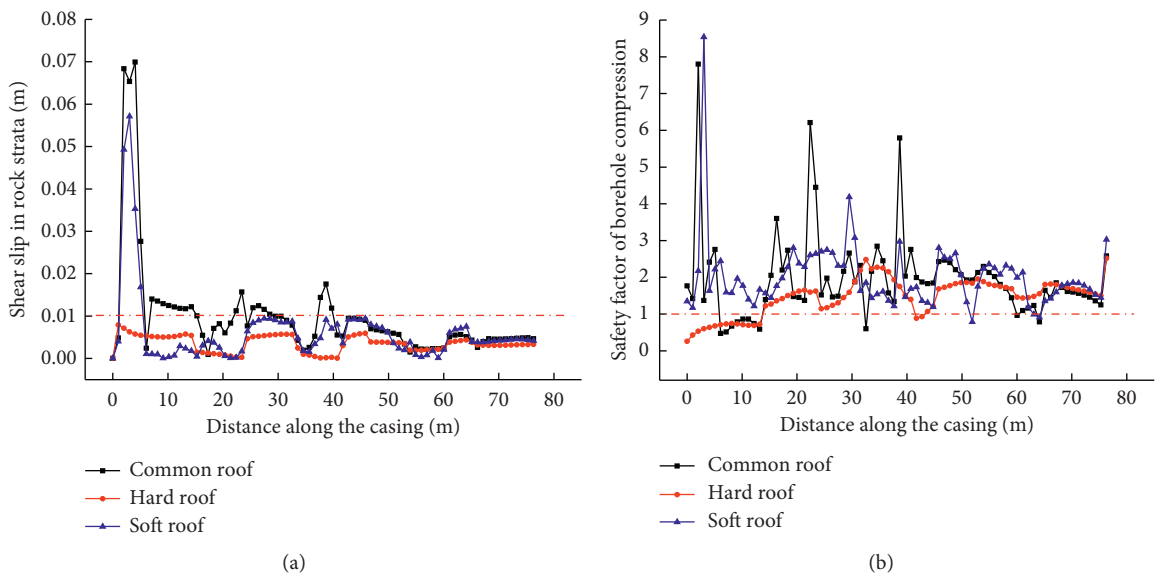

Figure 13: Effect of roof lithology on the stability of the borehole. (a) Effect of roof lithology on the shear stability of the borehole. (b) Effect of roof lithology on the compressional stability of the borehole.

4.6. Effect of Support Scheme on the Stability of Borehole. The variation rules of the borehole stability of the 2# drilling path with support schemes 1, 2, and 3 are shown in Figure 14. We conclude the following from the diagram:

(1) It can reduce the dangerous area and risk degree of borehole shear failure to strengthen the support strength of the retaining roadway, especially in lower strata. This is mainly because the subsidence of the roadway roof on the filling wall side is controlled by improving the supporting strength. Therefore, the interlayer shear slip is reduced. It can be concluded that the reinforcing support strength of "primary supports" in roadway retaining walls can decrease the difficulty associated with maintenance of "minor supports" of boreholes, to some extent.

(2) Strengthening the support strength also has a certain effect on the stability of the borehole compressional failure, but the effect is not significant with regard to the stability of borehole shear failure.

5. Field Test

As shown in Figure 1, we drilled a total of 11 drainage boreholes in three groups, sequentially, in CR 4, CR 3, and CR 2. Different protection measures were adopted in the drainage boreholes. To grasp the law of deformation and failure of drainage boreholes, a borehole camera exploration device was used to measure borehole stability during the advance of the face. After five months of monitoring, boreholes 1 through 8 were found to be broken, whereas boreholes 9 through 11, which had a dual thick-walled combined casing, did not fracture during the extraction. Details of the borehole failure position along the casing, the height into the roof, and the distance behind the coal face where the casing failed are shown in Figure 15.

From Figure 15, we conclude that boreholes were broken at a distance of 2–14 m behind the coal face, and 87.5% of that occurred over a distance of 9–14 m behind the coal face. The failure position of boreholes occurred at depths of 5–10 m along the casing, which were all in strata above the roadway roof at 4–9 m. The observed results are consistent with the numerical simulation, indicating that the proposed multidimensional coupling numerical simulation method can be used as an effective method for borehole design and protection.

6. Conclusions

Gas boreholes that penetrate mineable coal seams may be subject to distress caused by integrated mining coal and gas. The concentrated compressive stresses and the lateral shear offsets are especially important because they are the most damaging for boreholes. To reveal the space-time evolution characteristics and influence factors of fracture deformation of the gob-side gas boreholes, a multidimensional coupling numerical model that considers the combined effects of topography, various mining heights, and support schemes is presented based on the practice of deep thin coal seam pressure relief in the Huainan mining area. Through this study, the following conclusions are drawn:

(1) Results indicate that the danger zone for borehole fracturing is mainly in the scope of 5–12 m above the roof of the roadway. The final-hole position has little effect on the stability of boreholes, and migrating the open-hole position to the entity coal side and roadway roof side can improve the stability of the borehole. The initial failure of the borehole occurs at a distance of 10 m behind the coal face. The failure of the borehole is basically stable at a distance of 100–120 m behind the coal face.

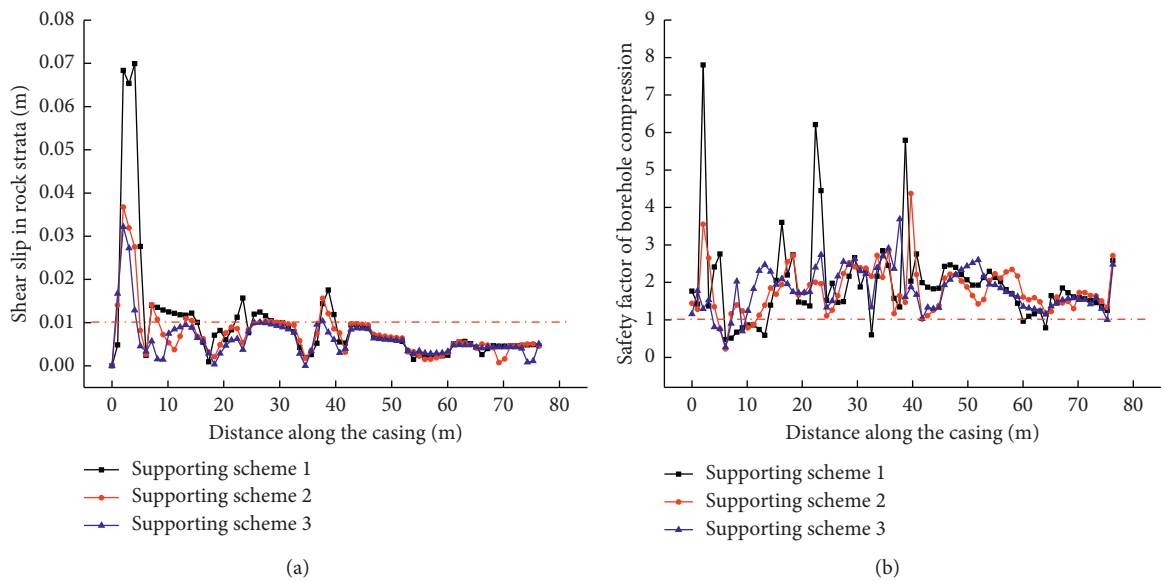

Figure 14: Effect of support scheme on the stability of the borehole. (a) Effect of support scheme on the shear stability of the borehole. (b) Effect of support scheme on the compressional stability of the borehole.

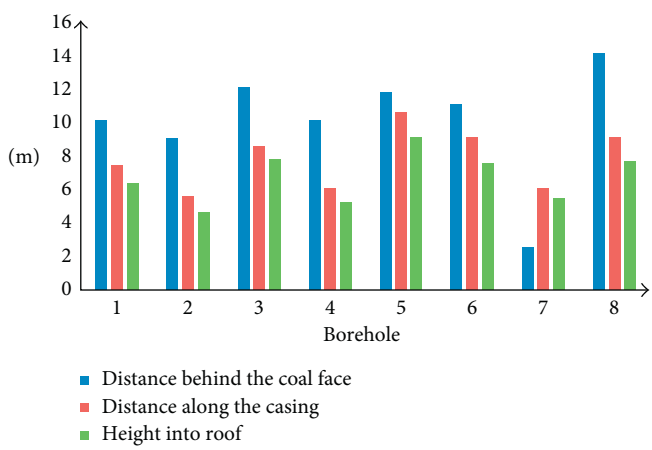

Figure 15: Data for borehole failure position along the borehole, height into the roof, and distance behind the coal face where the borehole failed.

(2) With an increase in mining height leading to an increase in the movement of strata and an increase in the range of pressure relief, the shear stability of the borehole is reduced and the extrusion stability of the borehole is improved. A hard roof condition promotes borehole shear stability; a weak roof condition promotes borehole extrusion stability. It can decrease the maintenance difficulty associated with "minor supports" in boreholes to some extent by reinforcing the support strength of "primary supports" in roadway-retaining walls.

(3) The tracing observation of the borehole stability during advance of the 11 test boreholes shows that borehole destruction occurs at a distance of 9–14 m behind the coal face, and the failure position of boreholes occurs at depths of 5–10 m along the casing. These results are consistent with the results of the numerical simulation analysis.

Data Availability

The readers can access the data supporting the conclusions of the study by sending a mail to the corresponding author of this paper, and all data can be coshared without restriction.

Conflicts of Interest

The authors declare that there are no conflicts of interest regarding the publication of this paper.

Acknowledgments

Financial support for this work was supported by the Collaborative Innovation Center for Prevention and Control of Mountain Geological Hazards of Zhejiang Province (PCMGH-2016-Y-05), Shaoxing Public Interest Research Projects (Grant no. 2017B70002), and the Research Start-Up Funding Project of Shaoxing University (no. 20165014).

References

[1] Y. Liang, "Key technique of safe mining in low permeability and methane-rich seam group," *Chinese Journal of Rock Mechanics and Engineering*, vol. 27, no. 7, pp. 1370–1379, 2008.

[2] Y. Liang, "The technique of coal mining and gas and borehole extraction by roadway retaining drilling," *Journal of China Coal Society*, vol. 33, no. 8, pp. 898–902, 2008.

[3] Y. Wu, Z. Pan, D. Zhang, Z. Lu, and L. D. Connell, "Evaluation of gas production from multiple coal seams: a simulation study and economics," *International Journal of Mining Science and Technology*, vol. 28, no. 3, pp. 359–371, 2018.

[4] L. Cheng, L. Shugang, and Y. Shouguo, "Gas emission quantity prediction and drainage technology of steeply inclined and extremely thick coal seams," *International Journal of Mining Science and Technology*, vol. 28, no. 3, pp. 415–422, 2018.

[5] C. Ö. Karacan, J. P. Ulery, and G. V. R. Goodman, "A numerical evaluation on the effects of impermeable faults on degasification efficiency and methane emissions during underground coal mining," *International Journal of Coal Geology*, vol. 75, no. 4, pp. 195–203, 2008.

[6] K. Noack, "Control of gas emissions in underground coal mines," *International Journal of Coal Geology*, vol. 35, no. 1, pp. 57–82, 1998.

[7] Z. Yong, Z. Xibin, X. Lifeng, Z. Jiangli, and Z. Genlia, "Formation and evolution of gas flow channels in the abutment pressure area," *International Journal of Mining Science and Technology*, vol. 22, no. 6, pp. 801–807, 2012.

[8] Y. Zhang, X. Zhang, C. Li, C. Liu, and Z. Wang, "Methane moving law with long gas extraction holes in goaf," *Procedia Engineering*, vol. 26, pp. 357–365, 2011.

[9] C Ö. Karacan, W. P. Diamond, and S. J. Schatzel, "Numerical analysis of the influence of in-seam horizontal methane drainage boreholes on longwall face emission rates," *International Journal of Coal Geology*, vol. 72, no. 1, pp. 15–32, 2007.

[10] T. H. Yang, T. Xu, H. Y. Liu, C.A. Tang, B. M. Shi, and Q. X. Yu, "Stress-damage-flow coupling model and its application to pressure relief coal bed methane in deep coal seam," *International Journal of Coal Geology*, vol. 86, no. 4, pp. 357–366, 2011.

[11] D. N. Whittles, I. S. Lowndes, S. W. Kingman, C. Yates, and S. Jobling, "The stability of methane capture boreholes around a long wall coal panel," *International Journal of Coal Geology*, vol. 71, no. 2-3, pp. 313–328, 2007.

[12] Y. Liu, T. Lu, and H. Yu, "Surface boreholes for drainage of goaf gases and its stability analysis," *Chinese Journal of Rock Mechanics and Engineering*, vol. 24, no. 1, pp. 4982–4987, 2005.

[13] H. Sun, Y. Zheng, Q. Hu, and F. Lin, "Surface borehole casing coupling deformation mechanism," *Journal of China Coal Society*, vol. 36, no. 5, pp. 823–829, 2011.

[14] H. Sun, F. Lin, J. Zhang et al., "Faculty of civil shear deformation model on surface drilling and its spatial analysis," *Journal of Mining & Safety Engineering*, vol. 28, no. 1, pp. 72–76, 2011.

[15] H. Sun, D. Liu, L. Liang et al., "Key rock strata effecting analysis on surface borehole shear deformation fracture," *Journal of Chongqing University*, vol. 32, no. 5, pp. 550–555, 2009.

[16] J. Chen, T. Wang, Y. Zhou, Y. Zhu, and X. Wang, "Failure modes of the surface venthole casing during longwall coal extraction: a case study," *International Journal of Coal Geology*, vol. 90-91, pp. 135–148, 2012.

[17] P. J. Périé, *Laboratory Investigation of Rock Fracture around Boreholes*, University of California, Berkeley, CA, USA, 1990.

[18] Y. Liu, F. Zhou, C. Liu et al., "Study and application of new bending and shearing resistant surface borehole structure," *Safety in Coal Mines*, vol. 38, no. 1, pp. 92–95, 2012.

[19] F. Wang, T. Ren, S. Tu, S. Tu, F. Hungerford, and N. Aziz, "Implementation of underground longhole directional drilling technology for greenhouse gas mitigation in Chinese coal mines," *International Journal of Greenhouse Gas Control*, vol. 11, no. 6, pp. 290–303, 2012.

[20] H. Guo, L. Yuan, B. Shen, Q. Qu, and J. Xue, "Mining-induced strata stress changes, fractures and gas flow dynamics in multi-seam longwall mining," *International Journal of Rock Mechanics & Mining Sciences*, vol. 54, no. 3, pp. 129–139, 2012.

[21] F. Xue, N. Zhang, X. Feng, X. Zheng, and J. Kan, "Strengthening borehole configuration from the retaining roadway for greenhouse gas reduction: a case study," *PLoS One*, vol. 10, no. 1, Article ID e0115874, 2015.

[22] N. Zhang, X. Xue, and F. Han, "Technical challenges and countermeasures of the co-excavation of coal and gas with no-pillar retains in deep coalmine," *Journal of China Coal Society*, vol. 40, no. 10, pp. 2251–2259, 2015.

[23] C. Xiaocun and T. Hui, "Technical scheme and application of pressure-relief gas extraction in multi-coal seam mining region," *International Journal of Mining Science and Technology*, vol. 28, no. 3, pp. 483–489, 2018.

[24] C. Liu, F. Zhou, K. Yang, X. Xiao, and Y. Liu, "Failure analysis of borehole liners in soft coal seam for gas drainage," *Engineering Failure Analysis*, vol. 42, no. 5, pp. 274–283, 2014.